Molecular Crystals and Liquid Crystals
Publication details, including instructions for authors and subscription information:
http://www.tandfonline.com/loi/gmcl20

Phase Organization of Mesogen-Decorated Spherical Nanoparticles

Silvia Orlandi [a] & Claudio Zannoni [a]
[a] Dipartimento di Chimica Industriale "Toso Montanari" , Università di Bologna, Viale Risorgimento , Bologna , Italy
Published online: 02 Apr 2013.

To cite this article: Silvia Orlandi & Claudio Zannoni (2013) Phase Organization of Mesogen-Decorated Spherical Nanoparticles, Molecular Crystals and Liquid Crystals, 573:1, 1-9, DOI: 10.1080/15421406.2012.763213

To link to this article: http://dx.doi.org/10.1080/15421406.2012.763213

Mol. Cryst. Liq. Cryst., Vol. 573: pp. 1–9, 2013

ISSN: 1542-1406 print/1563-5287 online
DOI: 10.1080/15421406.2012.763213

Taylor & Francis
Taylor & Francis Group

Phase Organization of Mesogen-Decorated Spherical Nanoparticles

SILVIA ORLANDI* AND CLAUDIO ZANNONI

Dipartimento di Chimica Industriale "Toso Montanari," Università di Bologna, Viale Risorgimento, Bologna, Italy

We present a Monte Carlo simulation study of the phase behavior and molecular organizations observed in a system of nanoparticles constituted by a central spherical core with attached mesogenic groups, which we model with a set of suitable Gay–Berne units connected by flexible spacers. We show that the choice of radial or tangential orientation of the attached mesogenic groups with respect to the surface of the core is crucial for the resulting phase behavior.

Keywords Computer simulation; mesogen-coated nanoparticles; Monte Carlo

1. Introduction

The anisotropy of the constituent particles, be it rodlike, calamitic or flatlike, discotic [1] has long been considered as necessary requirement for the formation of liquid crystal (LC) phases. This situation has recently changed with the discovery of a variety of LCs with shape deviating from these canonical shapes such as bent, "banana" [2,3], phasmidic [4], dendrimeric [5], fullerenic [6–9] mesogens.

A particularly striking case is that of spherical nanoparticles (NPs), typically gold ones, decorated with mesogens attached radially or tangentially with a flexible thiol-terminated spacer group to the gold surface [10–15]. These NPs are in some ways similar to first-generation dendrimers, and form various liquid crystalline phases.

Although simulations at space resolutions going from the mesoscopic scale, with positions arbitrarily fixed on lattices [16], to the molecular scale with off-lattice coarse grained [17] or even down to atomistic [18] level of detail exist for many mesogenic systems of various complexity [19–23], we are not aware of any modeling and simulation studies conducted to understand the phases and the ordering process in these exotic systems that, on the other hand, have many promising applications, for example, in the field of optical metamaterials, and more generally, in the field of novel functional materials with hybrid properties [24–27].

In this work, we intend to provide a first simple model to treat spherical NPs decorated, on the surface, with mesogens and study their phase behavior.

*Address correspondence to Silvia Orlandi, Dipartimento di Chimica Industriale "Toso Montanari," Università di Bologna, Viale Risorgimento 4, Bologna 40136, Italy. Fax: +39-051-2093690. E-mail: s.orlandi@unibo.it

2. Model and Simulation

We set out to implement the essential characteristic of two classes of NPs architectures, where the mesogens are attached to the central unit either at an end, that is, radially, or at a side, that is, tangentially (see Fig. 1).

Each model consists of one central sphere representing the NP core (N) and eight equivalent uniaxial Gay–Berne (GB) elongated ellipsoids representing the substituent mesogens (M). We assume that the spherical core site is connected to the mesogens through a flexible spring, with the bonding sites placed on surface of sphere and ellipsoids; bonds can only stretch and bend but not break during the simulation [28].

The corresponding bonded interactions are expressed with harmonic contributions depending on the separation $s_{ij} = |\mathbf{p}_j - \mathbf{p}_i|$, and the bending angle $\theta_{ij} = \cos^{-1}(\mathbf{u}_i \cdot \mathbf{u}_j)$ between two linked bonding sites:

$$U^{BND} = \varepsilon 0[k_s(s_{ij} - s_{eq})^2 + k_\theta(\theta_{ij} - \theta_{eq})^2] \tag{1}$$

where $\mathbf{p}$ and $\mathbf{u}$ are the positions and the orientations of the bonding sites, s_{eq} and θ_{eq} the equilibrium spacer length and bend angle, and k_s, k_θ the stiffness parameters of the spacer. For both the cases, we have used the same spacer, with bending harmonic constant $k_\theta = 100$ rad^{-2}, bond angle $\theta_{eq} = 180^\circ$, stretching harmonic constant $k_s = 200\,\sigma_0{}^{-2}$, and equilibrium length $s_{eq} = 0.5\,\sigma_0$.

Each of the sites on an NP, spherical (N) and mesogenic (M), interacts via a generalized GB repulsive-attractive site–site potential [17,29,30] and the potential between a pair of nine-site molecules is the sum of all possible interactions between the sites of two molecules, namely:

$$U^{GB} \equiv U^{GB}_{MM} + U^{GB}_{NN} + U^{GB}_{MN}. \tag{2}$$

The interaction potential is a special case of the expression developed for dissimilar biaxial particles A, B [31]:

$$\begin{aligned} U^{GB}_{AB}(\omega_A, \omega_B, \hat{\mathbf{r}}_{AB}) = 4\varepsilon_0 \varepsilon^{\nu}_{AB}(\omega_A, \omega_B, \hat{\mathbf{r}}_{AB}) \varepsilon'^{\mu}_{AB}(\omega_A, \omega_B, \hat{\mathbf{r}}_{AB}) \\ \times \left\{ \left[\frac{\sigma_c}{r_{AB} - \sigma_{AB}(\omega_A, \omega_B, \hat{\mathbf{r}}_{AB}) + \sigma_c} \right]^{12} \right. \\ \left. - \left[\frac{\sigma_c}{r_{AB} - \sigma_{AB}(\omega_A, \omega_B, \hat{\mathbf{r}}_{AB}) + \sigma_c} \right]^{6} \right\}, \end{aligned} \tag{3}$$

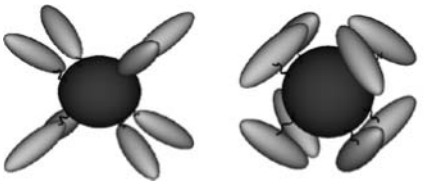

Site	σ_s	σ_e	σ_c	ε_s	ε_e	n_{bnd}
N	3.0	3.0	3.0	0.5	0.5	8
M	1.0	3.0	1.0	1.0	0.2	1

Figure 1. Schematic drawing of the radially (left) and laterally (right) grafted model nanoparticles. Dimensions and interaction parameters of the nanoparticle (N, dark gray) and mesogenic (M, light gray) interaction sites, expressed in terms of the parameters σ_0, ε_0 that serve to scale the simulation energy and distance units are reported in the table given in the figure.

where ω_A and ω_B are the molecular orientations in terms of Euler angles [29], $\mathbf{r}_{AB} \equiv \mathbf{r}_A - \mathbf{r}_B$ is the site–site vector, $\sigma_{AB}(\omega_A,\omega_B,\hat{\mathbf{r}})_{AB})$ anisotropic distance function and σ_c the minimum contact distance, $\varepsilon^{\nu}{}_{AB}(\omega_A,\omega_B,\hat{\mathbf{r}})_{AB})$ is the interaction strength at zero separation, and $\varepsilon'^{\mu}{}_{AB}(\omega_A,\omega_B,\hat{\mathbf{r}})_{AB})$ the ad-hoc interaction term as defined in [31], containing the empirical exponents μ and ν, used for tuning the potential angular dependence, that we select respectively equal to 1 and 3.

This expression is a generalized version of the GB potential, which can be used for a straightforward calculation of the mixed interaction potential between dissimilar particles A, B by simply employing $\sigma_c = \frac{1}{2}\left[\sigma_c^A + \sigma_c^B\right]$.

Actually the GB potential depends only on the ratios of the sigmas and the epsilons that we choose as $\sigma_e/\sigma_s = 1$ and $\varepsilon_s/\varepsilon_e = 1$ for the N (spherical) site and $\sigma_e/\sigma_s = 3$ and $\varepsilon_s/\varepsilon_e = 5$ for the M (rod-like) site (see Fig. 1) where s and e stand for side-to-side and end-to-end dimer arrangements. The parameterization for the M sites in case of systems of uniaxial ellipsoid particles gives a broad temperature range of nematic, smectic, and crystal phases [17,28,30,32].

We performed a large number of Monte Carlo (MC) experiments in the isobaric-isothermal (*NPT*) ensemble, at adimensional pressure $P^* \equiv P\sigma_0{}^3/\varepsilon_0 = 5$ and temperature $T^* \equiv k_B T/\varepsilon_0$, on samples of $N = 125$ decorated NPs (i.e., 125 spherical sites and 1000 rod sites).

For both radial or tangential attachment types, simulations started from well-equilibrated configurations in the isotropic phase. The simulations were run in a cooling-down sequence of MC runs, each of them starting from the final equilibrated configuration obtained at the previous temperature. The length of equilibration MC runs varied starting from 0.5 millions cycles, for the first isotropic configurations, to 1.0 million cycles on the approach of ordered phases at lower temperatures, each cycle corresponding to N attempted single-particle MC moves and the acceptance ratio being 0.4. From a practical point of view, we have used an orthogonal simulation box with three-dimensional periodic boundary conditions, allowing its sides to fluctuate independently during the MC evolution so as to let the system adjust to its equilibrium density at the given thermodynamic state and to help avoiding formation of cavities in the sample. During production run, thermodynamic observables have been accumulated for averaging and data analysis every 20 cycles.

The average values of dimensionless energy $\langle U^* \rangle$and order parameter $\langle P_2 \rangle = \langle \frac{3}{2}(\hat{\mathbf{z}}_i \cdot \hat{\mathbf{Z}})^2 - \frac{1}{2} \rangle$, showing the average orientational order of the molecular $\hat{\mathbf{z}}_i$ axis with respect to the director orientation defining unit vector $\hat{\mathbf{Z}}$, were determined from the simulations.

Characterization of the phase was accomplished first by calculating density correlation functions along the director (along Z axis) and perpendicular to it (XY plane rod–rod and sphere–sphere correlation functions) for both M and N sites:

$$g_{||}(r) = \frac{1}{\pi R_{||}^2 \rho} \langle \delta|(\mathbf{r} - \mathbf{r}_{ij}) \cdot \mathbf{Z}| \rangle_{ij} \equiv \frac{1}{\pi R_{||}^2 \rho} \langle \delta(z - z_{ij}) \rangle_{ij} \tag{4}$$

$$g_{\perp}(r) = \frac{1}{\pi R_{\perp}^2 \rho} \langle \delta|(\mathbf{r} - \mathbf{r}_{ij})| \times \mathbf{Z} \rangle_{ij}, \tag{5}$$

which give the probability to find a molecule respectively in a layer perpendicular to the director and in cylindrical shells having as axis the director ($R_{\parallel}$ and $R_{\perp}$ are the radii of the corresponding sampling regions). All the two particles averages $< \ldots >$ij are computed

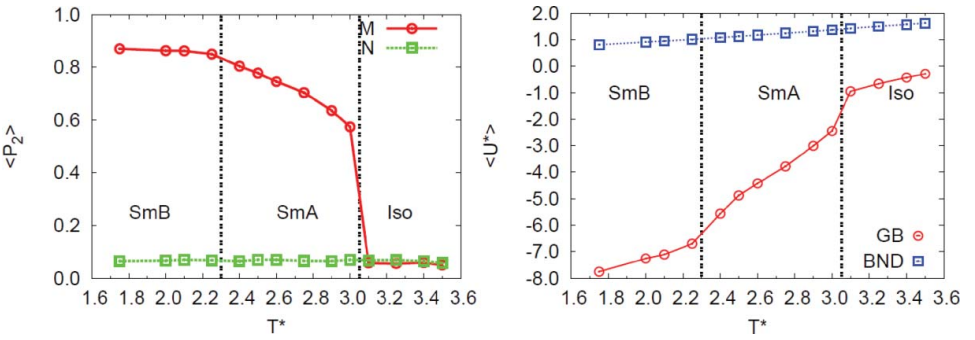

Figure 2. Orientational order parameter $\langle P_2 \rangle$ and average energy $\langle U^* \rangle$ per decorated nanoparticle with radial substitution, as a function of T^*, at dimensionless pressure $P^* = 5$.

over all molecular pairs and configurations. The density correlation function $g_{||}(r)$ is particularly useful for the identification of the layered structures present in the systems, while the $g_{\perp}(r)$ is helpful for investigations of the order inside the layers and gives the information about the positional order of spherical and rod sites.

3. Results

Temperature dependence profiles of the main observables of the two studied systems, with radial and tangential substitution, that is, average energy per decorated nanoparticle and orientational order parameter $\langle P_2 \rangle$, at pressure $P^* = 5$, are reported in Figs. 2 and 5. Chosen snapshots presenting molecular assemblies obtained in simulations are given in Figs. 3 and 6, while correlation functions in Figs. 4 and 7.

Simulations show that, upon decreasing temperature, the system with radial substitution undergoes phase changes accompanied by an increase of orientational and translational

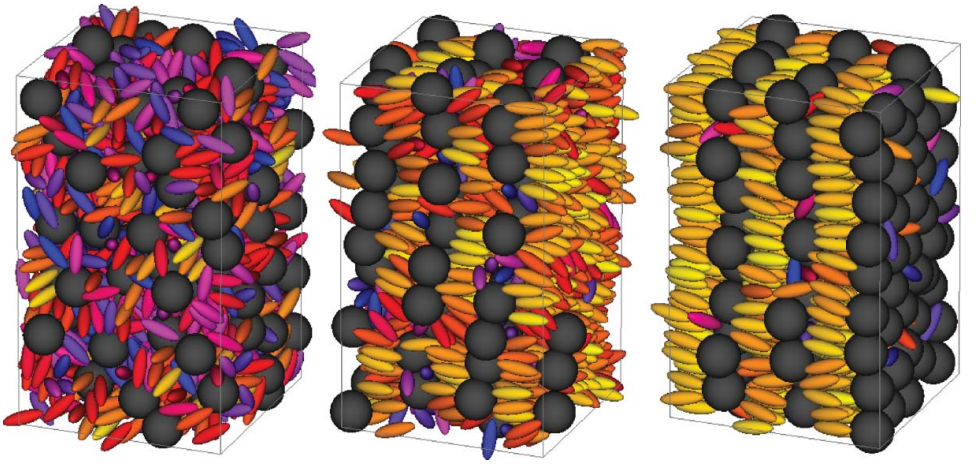

Figure 3. Snapshots of samples of 125 radially grafted nanoparticles at $T^* = 3.2$ (Nematic), 3.0 (Smectic A), 2.0 (Smectic B). Dimensionless pressure is $P^* = 5$. The spherical central nanoparticle is represented by a dark gray sphere, while mesogens are color coded according to their orientation.

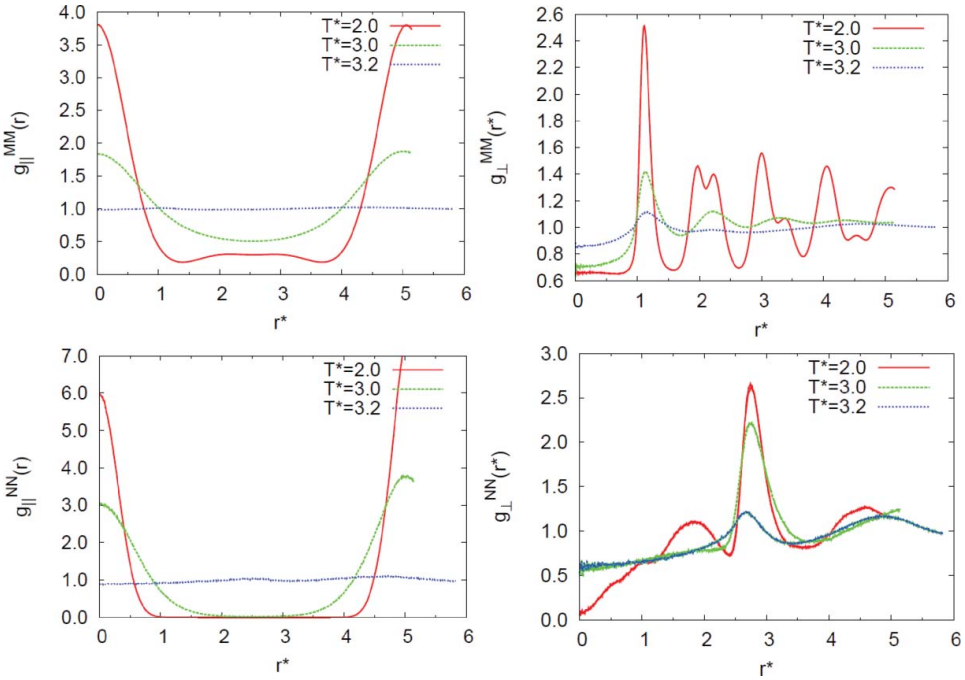

Figure 4. Density correlation function along the director and perpendicular to it for the system with radial substitution at three temperatures corresponding to Isotropic ($T^* = 3.2$, dashed line), Smectic A ($T^* = 3.0$, dotted lines), Smectic B ($T^* = 3.2$, solid line) phases.

order with Isotropic, Smectic A, and Smectic B phases. Quite interestingly, even in the range of temperatures 3.0−2.7, characterized by orientational order parameter typical of nematic phases, we observe a strong structuration in layers for both M and N sites, as indicated by the density correlation functions along the director $g_{||}^{NN}(r)$ and $g_{||}^{MM}(r)$ (see Fig. 4).

Both functions show a sharp modulation, suggesting that spheres and rods are arranged in sublayers; maxima are separated by the distance $r^* \approx 5.0$ (roughly half of decorated NP in the linear conformation) that implies a fully interdigitated structure of the mesogenic layers.

The existence of this phase organization is supported by the snapshots of equilibrated configurations reported in Fig. 3: at the lowest temperatures, the mesogenic groups tend to align with each other and to segregate at the two ends of the spherical NP, enhancing phase separation, as a microsegregation of both M and N sites in continuous quasi-planar sublayers is observed.

From the correlation functions in the direction perpendicular to the director in the sublayer made of cores, $g_{\perp}{}^{NN}$, and in the sublayer made of mesogens, $g_{\perp}{}^{MM}$, it can be noticed (see Fig. 4) that the rod-like units exhibit higher positional order than the spherical ones. In particular, at $T^* = 2.0$ the characteristic splitting of the second peak around $r^* \cong 2.0$ is evident, indicating a hexagonal order typical of Smectic B phases; while, at the intermediate temperature $T^* = 3.0$, the rapid decay of the density correlation and the lack of double peaks highlight the liquid-like order inside the layer, characteristic of Smectic A phases.

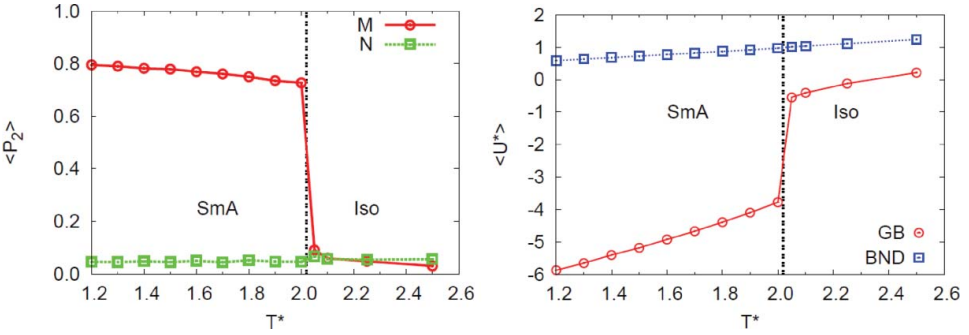

Figure 5. Orientational order parameter $\langle P_2 \rangle$ and average energy $\langle U^* \rangle$ per decorated nanoparticle with tangential substitution, as a function of T^*, at dimensionless pressure $P^* = 5$.

Turning to the model with tangentially attached mesogenic groups, our simulations show that the system yields mesomorphism with Isotropic and Smectic A phases. Comparing with the radially attached model, we observe a general reduction of the liquid crystalline orientational order parameter $\langle P_2 \rangle_M$ and a shift to lower temperatures of the Isotropic-Smectic A transition (Fig. 5).

The density correlation functions along the director for the mesogenic sites, $g_{\parallel}{}^{MM}(r)$, show, in smectic phase, a modulation with maxima separated by the distance $r^* \approx 2.7$; instead, and differently from the radially substitution case, the $g_{\parallel}{}^{NN}(r)$ shows a more complicated structure of peaks with maxima still separated by $r^* \approx 2.7$.

Correspondingly, the snapshots of typical molecular organizations obtained from simulations, even at the lowest temperature (see Fig. 6), evidence that the central spherical cores no longer organize in continuous planes, but rather are packed in columnar stacks separated by a distance $r^* \approx 4.0$ and regularly arranged in the whole box volume. On the other hand, mesogenic sites still tend to organize in layers, even if discontinuous.

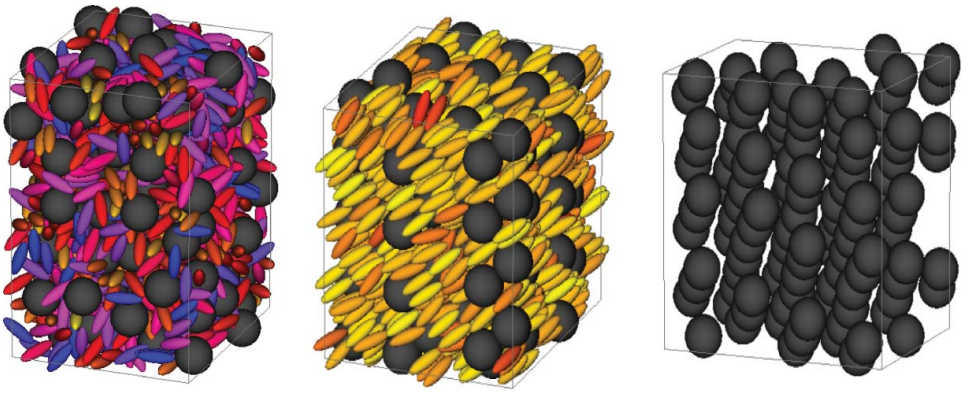

Figure 6. Snapshots of molecular organizations of the 125 laterally grafted nanoparticles sample at $T^* = 2.2$ (left), and 1.8 (center). The spherical central nanoparticle is represented by a dark gray sphere, while mesogens are color coded according to their orientation. To help in the visualization of the columnar stacks, only the spherical sites have been represented and a top view has been chosen for the snapshot on right, relative to temperature $T^* = 1.8$.

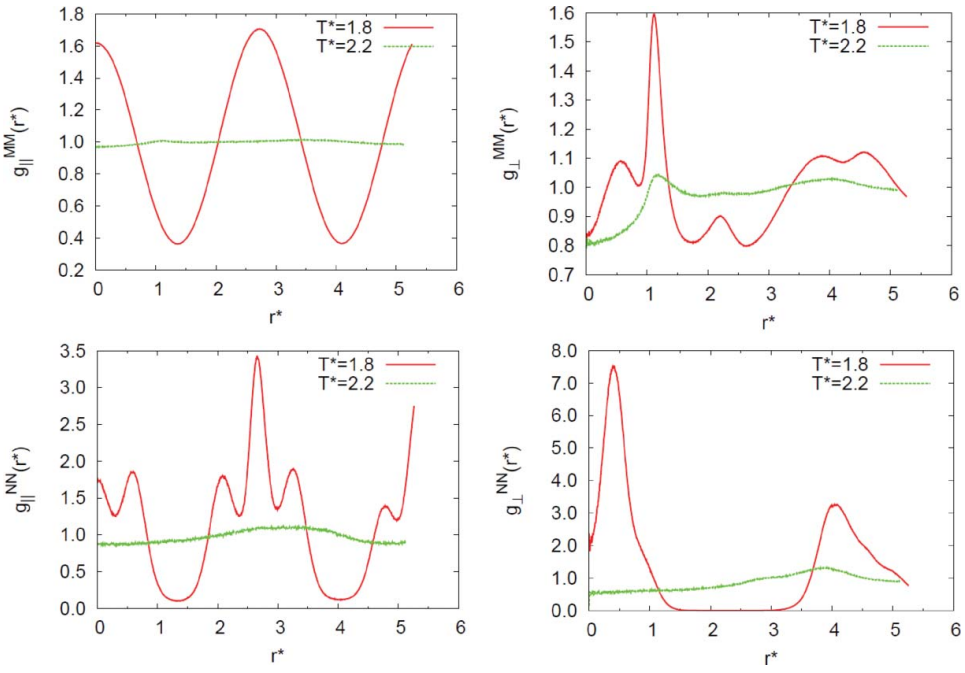

Figure 7. Density correlation function along the director and perpendicular to it for the system of nanoparticles with tangential substitution in Isotropic ($T^* = 2.2$, dashed line) and in Smectic A ($T^* = 1.8$, solid line) phases.

Trying to rationalize this molecular arrangement, we observe that for the tangential substitution, the bonded mesogens cannot migrate at the two ends of the spherical NP, and remain distributed over its surface; thus, the linear conformation, and consequently the spheres segregation are prevented.

4. Conclusions

We have studied, by means of MC simulations, the molecular organizations for two classes of NP architectures with mesogens attached to the central spherical core in a radial or in a tangential way.

The simulations show that upon lowering temperature, the system with radial substitution yields microsegregation of both spherical and mesogenic sites with consequent formation of quasi-planar sublayers; the system with lateral substitution gives a very different aggregation patterns with spherical sites segregate both into regularly packed columnar stacks and in (discontinuous) layer. The internal flexibility appears essential for this peculiar self-assembling feature. Even though this is a very simple model for mesogen-decorated NPs, and thus a detailed comparison with experiment would probably be inappropriate at this stage, since no attempt has been made to tune NP size, spacer length, and number of mesogenic ligands, it is comforting to see that the striking observation of LC phases formation for these unconventional shaped particles is reproduced and that the organization found is quite similar to what has been assumed in experimental work [10–16,24].

Acknowledgments

We thank MIUR PRIN national project "Novel ordered systems for high response molecular devices" (2009N5JH4F) for financial support.

References

[1] Blinov, L. (2011). *Structure and Properties of Liquid Crystals*, Springer: Dordrecht.
[2] Link, D. R., Natale, G., Shao, R., Maclennan, J. E., Clark, N. A., Korblova, E., & Walba, D. M. (1997). *Science*, *278*, 1924–1927.
[3] Francescangeli, O., Stanic, V., Torgova, S. I., Strigazzi, A., Scaramuzza, N., Ferrero, C., Dolbnya, I. P., Weiss, T. M., Berardi, R. Muccioli, L., Orlandi, S., & Zannoni, C. (2009). *Adv. Funct. Mater.*, *19*, 2592–2600.
[4] Yoon, S. J., Kim, J. H., Kim, K. S., Chung, J. W., Heinrich, B., Mathevet, F., Kim, P., Donnio, B., Attias A. J. Kim, D., & Park, S. Y. (2012). *Adv. Funct. Mater.*, *22*, 61–69.
[5] Donnio, B., Buathong, S., Bury, I., & Guillon, D. (2007). *Chem. Soc. Rev.*, *36*, 1495–1513.
[6] Deschenaux, R., Donnio, B., & Guillon, D. (2005). *New J. Chem.*, *31*, 1064–1073.
[7] Bushby, R. J., Hamley, I. W., Liu, Q. Y., Lozman, O. R., & Lydon, J. E. (2005). *J. Mat. Chem.*, *15*, 4429–4434.
[8] Sawamura, M., Kawai, K., Matsuo, Y., Kanie, K., Kato, T., & Nakamura, E. (2002). *Nature*, *419*, 702–705.
[9] Chuard, T., Dardel, B., Deschenaux, R., & Even, M. (2000). *Carbon*, *38*, 1573–1576.
[10] Cseh, L., & Mehl, G. H. (2006). *J. Am. Chem. Soc.*, *128*, 13376–13377.
[11] Cseh, L., & Mehl, G. H. (2007). *J. Mat. Chem.*, *17*, 311–315.
[12] Mang, X. B., Zeng, X. B., Tang, B. J., Liu, F., Ungar, G., Zhang, R. B., Cseh, L., & Mehl, G. H. (2012). *J. Mat. Chem.*, *22*, 11101–11106.
[13] Wojcik, M. M., Gora, M., Mieczkowski, J., Romiszewski, J., Gorecka, E., & Pociecha, D. (2011). *Soft Matter*, *7*, 10561–10564.
[14] Wojcik, M., Kolpaczynska, M., Pociecha, D., Mieczkowski, J., & Gorecka, E. (2010). *Soft Matter*, *6*, 5397–5400.
[15] Wojcik, M., Lewandowski, W., Matraszek, J., Mieczkowski, J., Borysiuk, J., Pociecha, D., & Gorecka, E. (2009). *Angew. Chem. Int. Ed.*, *48*, 5167.
[16] Pasini, P., Chiccoli, C., & Zannoni, C. (2001). Liquid crystal lattice models. I. Bulk systems. In: P. Pasini & C. Zannoni (Eds.), *Advances in the Computer Simulations of Liquid Crystals*, Kluwer: Dordrecht, 2000, 5, 99.
[17] Zannoni, C. (2001). *J. Mat. Chem.*, *11*, 2637–2646.
[18] Tiberio, G., Muccioli, L., Berardi, R., & Zannoni, C. (2009). *Chem. Phys. Chem.*, *10*, 125–136.
[19] Ilnytskyi, J. M., Neher, D., Saphiannikova, M., Wilson, M. R., & Stimson, L. M. (2008). *Mol. Cryst. Liq. Cryst.*, *496*, 186.
[20] Ilnytskyi, J. M., Lintuvuori, J. S., & Wilson, M. R. (2010). *Cond. Matter Phys.*, *13*, 33001–3301.16.
[21] Sazonovas, A., Orlandi, S., Ricci, M., Zannoni, C., & Gorecka, E. (2006). *Chem. Phys. Lett.*, *430*, 297–302.
[22] Ellison, L. J., Michel, D. J., Barmes, F., & Cleaver, D. J. (2006). *Phys. Rev. Lett.*, *97*, 237801.
[23] Bates, M. A., & Walker, M. (2011). *Liq. Cryst.*, *38*, 1749–1757.
[24] Nealon, G. L., Greget, R., Dominguez, C., Nagy, Z. T., Guillon, D., Gallani, J. L. & Donnio, B. (2012). *Beilstein. J. Org. Chem.*, *8*, 349–370.
[25] Qi, H., & Hegmann, T. (2008). *J. Mat. Chem.*, *18*, 3288–3294.
[26] Lagerwall, J., & Scalia, G. (2012). *Curr. Appl. Phys.*, *12*, 1387–1412.
[27] Dintinger, J., Tang, B. J., Zeng, X., Kienzler, T., Mehl, G. H., Ungar, G. G., Rockstuh, C., & Scharf, T. (2012). *Proc. SPIE*, *8271*, 827106.
[28] Orlandi, S., Muccioli, L., Ricci, M., & Zannoni, C. (2009). *Soft Matter*, *5*, 4484–4491.

[29] Gay, J. G., & Berne, B. J. (1981). *J. Chem. Phys.*, *74*, 3316–3319.
[30] Berardi, R., Emerson, A. P. J., & Zannoni, C. (1993). *J. Chem. Soc. Faraday Trans.*, *89*, 4069–4078.
[31] Berardi, R., Fava C., & Zannoni, C. (1998). *Chem. Phys. Lett.*, *89*, 8–14.
[32] Berardi, R., Micheletti, D., Muccioli, L., Ricci, M., & Zannoni, C. (2004). *J. Chem. Phys.*, *121*, 9123–9130.